Design of a High Frequency Equal Width Annular Array Transducer for Medical Imaging

Y. Qian[1] and **N. R. Harris**[1],

ABSTRACT

This work investigates a strongly-focused annular array for high frequency ultrasonic applications, offering improved resolution without increasing the operating frequency, potentially reducing the complexity of manufacture. However, the conventional geometry, specifically the Equal Area array exhibits a problem with high sidelobes. A method based on geometric change is developed to control the lobe and leads to the design of an Equal Width annular array. This array successfully controls the sidelobe, and maintains the resolution improvement offered by strongly-focused arrays.

1. INTRODUCTION

Annular arrays have been used in high frequency ultrasonic (HFU) transducers for medical imaging requiring fine resolution, such as ophthalmology and dermatology [1, 2]. Most annular arrays published so far have an f-number around 2, and operating frequencies from 30 to 50 MHz [1-5]; a resolution of around 100 μm then can be provided. Increasing the operating frequency could further improve the resolution, but no annular array operating above 80 MHz has been reported. This is due to the poor penetration depth for the ultrasonic waves propagating into the fluid medium [6], while the very fine transducer structure also causes difficulties in fabrication [7].

In this paper, an alternative method is used to increase the resolution by reducing the f-number. This has the same effect as the increase of operating frequency, but at the cost of a reduced depth of field (DOF). The shortcoming in DOF can be overcome by dynamic focusing techniques as used in array transducers [8]. However, a major disadvantage of strongly-focused (or small f-number) annular arrays is found to be the relatively high sidelobes, which causes imaging artifacts [9].

Annular arrays usually consists of several concentric elements of the same area driven independently, namely an equal area (EA) array. EA arrays allow the same phase shift and impedance for every element; this offers a simplified design for driving/receiving circuits, but the outer elements are found to be implicated in the formation of high sidelobes when strongly focused arrays are designed. Therefore, an annular array with each element sharing the same width, the equal width (EW) array, is developed to suppress the unwanted sidelobe. Although this geometry negates the equal impedance and phase shift of each element and leads to more complex driving/receiving circuits, this is offset by the critical advance in the constraint of sidelobe as a key parameter for imaging. Although the resolution of EW arrays is slightly lower than equivalent EA arrays, there is still a good improvement compared to the conventional (or non-strongly-focused, f-number > 2) arrays.

Manuscript received on March 26, 2013 ; revised on November 25, 2013.

[1]School of Electronics and Computer Science, University of Southampton, University Road, SO17 1BJ Southampton, UK, email: nrh@ecs.soton.ac.uk

2. SIDELOBES IN EQUAL AREA ANNULAR ARRAY

An EA annular array is investigated initially. The design of the ceramic, matching and backing layer in this transducer follows the design guidelines well-studied by previous researchers [9], and Fig. 1 shows the schematic cross section of the transducer. Thus it can be calculated that the thickness of the *PZ34* layer is about 75 μm, and the quarter-wave matching layer is about 27 μm. By considering Fig. 4(a) which shows a typical pattern, it can be seen that the active layer of the array needs to be formed into annular elements, by for example laser micromachining, and the *kerfs* or grooves are then filled with an epoxy. The *kerf* width is set to be 20μm, a level that can be achieved by current dicing techniques [2,11]. Table 1 then lists the key parameters of the materials used for these layers and the *kerf* filler, where Z and c_L are the acoustic impedance and longitudinal sound speed, respectively.

The f-number of the array is set to be 1, instead of the conventional value of 2. Equation (1) gives the relationship between resolution R_L, operating frequency f_0 and f-number f, where c is the sound speed in the fluid (or water, $c \approx 1500$ m/s). It can be found that a conventional 30 MHz EA array with f-number of 2 is expected to offer a resolution of 100 μm, while one with an f-number of 1 could have a much finer resolution of 50 μm.

$$R_L = \frac{c}{f_0} \cdot f \tag{1}$$

The radiation of this annular array is then evaluated by FEA (Finite Element Method) using ANSYS

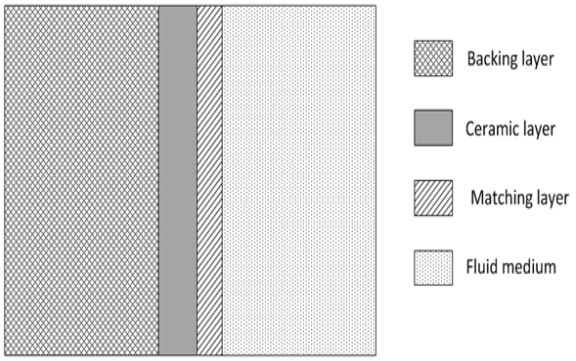

Fig.1:: Cross-section of a typical transducer

Table 1:: Key parameters of the materials used in the transducer

Layer	Material	Ref.	Z (MRayls)	c_L (m/s)
Matching	Alumina-loaded EPO-TEK 301-2	[12]	7.3	3248
Ceramic	PZ34	[7]	35.4	4661
Backing	Tungsten-loaded E-solder 3022	[12]	10	1600
Kerfs filler	Araldite	[12]	2.5	2210

11.0 with an element size of $\frac{\lambda}{8}$ after a mesh refinement study was carried out. FEA simulation has been demonstrated to show very similar responses to experimental results by many previous researchers, see for example [13]. The radiation pattern at the focal plane can be represented by the amplitude responses along a line drawn from the focal point at the plane due to the axis-symmetric geometry, as illustrated in Fig. 2.

The resolution is measured as the -6 dB full beam width and found to be about 55 μm, showing a good agreement to the theoretical value of 50 μm given

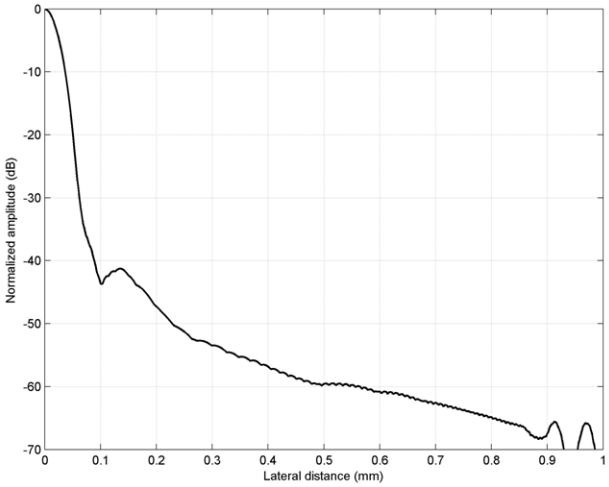

Fig.2:: Radiation pattern of the EA array calculated by FEA

by Equation 1. However, a sidelobe as high as -40 dB can be seen about 0.15 mm away from the focal point. For imaging it is recommended that this be below -50 dB to avoid any artefacts. Therefore, the high sidelobe needs to be suppressed for this type of strongly-focused annular array.

3. SIDELOBE ANALYSIS

This high sidelobe is found to be related to the geometry of the array elements. The Rayleigh integral, a good estimator to evaluate the radiation produced by an ideal piston [9], is used to analyze the sidelobe formation. Equation 2 then expresses the pressure response *p(r,t)* in the radiation field, where r is the vector representing the location of a point in the radiation field, and t denotes the time; *g(r_0,t)* here is a function to represent the pressure pulses emitted from a point in the array aperture, and r_0 similarly is a vector to describe the location of this point; *dS* here is the area element in the array aperture.

$$p(\vec{r},t) = \rho_0 \cdot \int_S \frac{g(\vec{r_0}, t - t_d)}{2\pi R} dS \qquad (2)$$

Two factors are found to be crucial to determine the pressure p; one is the distance R between a point at the focal plane to another one at the array aperture; and the other one is the total time delay t_d to describe the different arrival times for the pulses from the array aperture to reach a point in the radiation field.

The pattern is obtained by the summation of all the pulses travelling from the element aperture to the radiation field. However, it is hard to analyse the influence of each element on sidelobe formation because there are numerous pulses involved across the width of each element. Therefore, a simple assumption is made–the pulses of every element are represented by the pulse at its centre point R_c, as is illustrated in Fig. 3. Here the factor R is also displayed.

It should be noticed that every element is an annulus and actually shows two centre points in the cross-section, except the 1^{st} element, namely both the right and left centres are displayed in Fig. 3. To represent both the two centre points, subscript N and -N are introduced, where N is the element number. The positive N represents the right centres of the annular element, while the negative N denotes the left ones. However, since 1^{st} element only has one centre, the condition, $R_{c(1)}$=$R_{c(-1)}$=0 is defined. In addition, F_1 is the focal point with its coordinate (0, F), while the off-axis point F_2 is set to have the coordination (r_f, F), here r_f denotes distance away from the focal axis and F is focal distance.

Although this assumption may be too simple to offer good accuracy, it can be used to reveal the relationship between element pulses and sidelobe formation. The two factors R and t_d determine the pulse of every element at a certain point F_2 in the focal plane, of which the expressions are expressed as follows. Here φ_{dN} is the total phase shift, c is sound

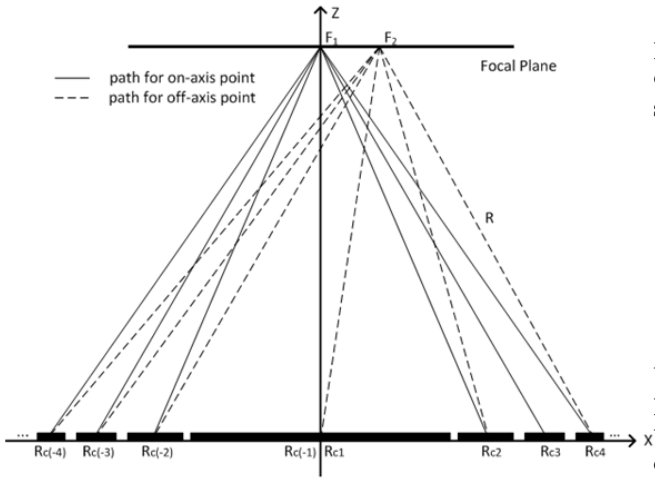

Fig.3:: The cross section of an EA annular array to focus in the medium

speed of water, and t_{fN} denotes the time delay applied into every element for focusing purposes.

$$t_{dN} = R_N/c + t_{fN}; \qquad \varphi_{dN} = T_{dN} \cdot 2\pi f \tag{3}$$

$$R_N = |F_2 - R_{cN}| = \sqrt{(r_f - R_{cN})^2 + F^2} \tag{4}$$

The value of r_f is set to be 140 μm, which is the position of the sidelobe for this 1 mm, 5 element, 30 MHz equal area annular array. It is found that the distance R_N for every element centre is very close to each other, in other words, the influence of factor R is not significant in the formation of this sidelobe.

However, the very small change in distance R might cause large change in time delay t_d or phase shift φ_d. By using Equation (3) and (4), t_d and φ_d are calculated but are found to be very large values that are hard to analyse. Therefore, another parameter namely the phase difference φ_{dif} is introduced and defined as the difference of φ_d for the two adjacent elements, likewise, the time difference t_{dif} is also defined, as expressed by Equation 6.

$$\begin{aligned} \varphi_{dif(N)} &= \varphi_{dN} - \varphi_{d(N-1)}; \\ t_{dif(N)} &= t_{dN} - t_{d(N-1)} \end{aligned} \tag{5}$$

Notice that the undefined φ_{d0} appears when N=0 and 1 in the above equations, hence, it is assumed that $\varphi_{d0} = \varphi_{d1} = \varphi_{d(-1)}$. This assumption leads to a phase/time difference of 0 for the central element; it physically means that the single centre point of 1^{st} element does not show any phase or time difference. With a given r_f of 140 μm, the values of φ_{dif} are listed in Table 2.

It can be seen that the outer elements show relatively close phase difference. It means that the pulses from outer elements could have a strong coherence in the sidelobe region. For the inner elements, the opposite is true–the relatively large phase difference between the inner elements suggests a complicated pulse overlapping or suppression, but at least no strong superposition is apparent.

Table 2:: Phase difference φ_{dif} of every element pulse at off-axis point (r_f, F); subscript N and N denote the right and left parts of each element, respectively

EA Element	1^{st}	2^{nd}	3^{rd}	4^{th}	5^{th}
$\varphi_{dif(N)}(^0)$	0	-254.5	-80.9	-63.4	-52.8
$\varphi_{dif(-N)}(^0)$	0	-242.0	-72.2	-55.2	-45.3

However, Table 2 only shows the intensity of pulse overlap from the nearby elements; the phase difference between left and right parts of the array element also impact the overlap. This difference is calculated by $\varphi_{d(N1)}$ - $\varphi_{d(N2)}$, where subscript N_1 and N_2 are the number of the element in either the left or right part. The smallest phase difference is found between $\varphi_{d(2)}$ and $\varphi_{d(-2)}$ showing the value about 300°, while the largest value is between $\varphi_{d(7)}$ and $\varphi_{d(-7)}$ with the value of 820° approximately. Since the pulses from array elements are usually very short, the phase difference ranging from 300° to 820° is large enough to separate the pulses from either suppression or overlap. In other words, the pulse overlap in the sidelobe region only depends on one part of the array, either left or right.

To summarize, the close phase difference of the pulses emitted from outer elements is likely to be the main source of the high sidelobe. A method is now developed to enlarge the phase difference, or equivalently reduce the pulse overlap in outer elements to suppress the sidelobe.

4. EQUAL WIDTH ANNULAR ARRAY

The separation of these phase differences could effectively decrease the pulse overlapping. The Fresnel approximation defined in Equation (6) is used with Equation (3) to show the relation between phase and the element.

$$\rho = \sqrt{X^2 + Y^2} = Y + X^2/2Y \tag{6}$$

The approximation is always valid when Y >> X. Thus by using the Fresnel approximation on distance R given by Equation (4), where the condition of "$F >> |r_f - R_{cN}|$" is generally valid, Equation (3) is transferred into the following form, where T_0 is a constant regardless of R_{cN}.

$$t_{dN} = T_0 - \frac{r_f \cdot R_{cN}}{F_c}; \qquad \varphi_{dN} = t_{dN} \cdot 2\pi f \tag{7}$$

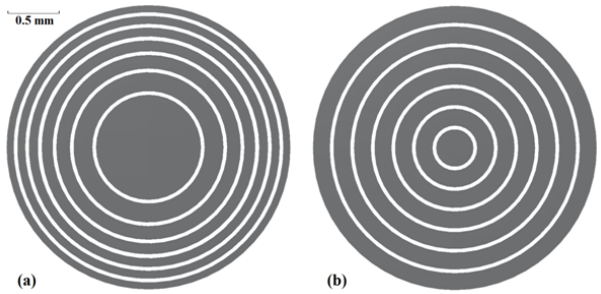

Fig.4:: The front view of (a) an EA array and (b) EW array

Table 3:: Phase difference φ_{dif} of the pulse in every EW element at off-axis point F_2 (r_f, F)

EA Element	1^{st}	2^{nd}	3^{rd}	4^{th}	5^{th}
$\varphi_{dif(N)}(^0)$	0	-150.4	-98.0	-93.1	-86.2
$\varphi_{dif(-N)}(^0)$	0	-145.9	-90.5	-83.0	-74.7

It can be found that the phase shift of the pulses at the point F_2 (F, r_f) only depends on R_{cN}, namely the element position.

Therefore, the close phase difference in the outer elements of the EA array is ascribed to the proximity of adjacent centre positions R_c. The separation of the element centre could lead to increasing phase shifts and less pulse overlap, resulting in improved sidelobe suppression. An equal width (EW) annular array can thus be developed, in which its elements in either left or right parts all share the same width. Notice that the width of 1^{st} element is assumed to be its radius due to the axis-symmetric structure. Fig. 4 displays the difference between EA and EW array.

Similar to Table 2, Table 3 lists the phase difference between adjacent elements in the EW annular array, including both left and right part. It is seen that the phase differences in outer elements increases to $-90°$ approximately, this is much larger than for the EA array. The strong overlap from outer elements in the EA array could therefore be reduced in the EW array. In addition, although the phase differences between the inner elements of the EW array become smaller, their values are still relatively large and pulse overlap will not be a problem. The high sidelobe seen the EA array is therefore expected to be reduced in the EW array.

In this EW annular array, only the geometry is changed compared to the EA array, all other parameters including transducer dimension and material remain the same. FEA is again used to evaluate the radiation pattern of the EW array, as illustrated in Fig. 5.

It can be seen that the sidelobe located at 140 μm in the EA array is clearly suppressed by using the EW geometry. However, another lobe appears far away from the focal axis in the radiation pattern of the EW array. This is found to be very similar to

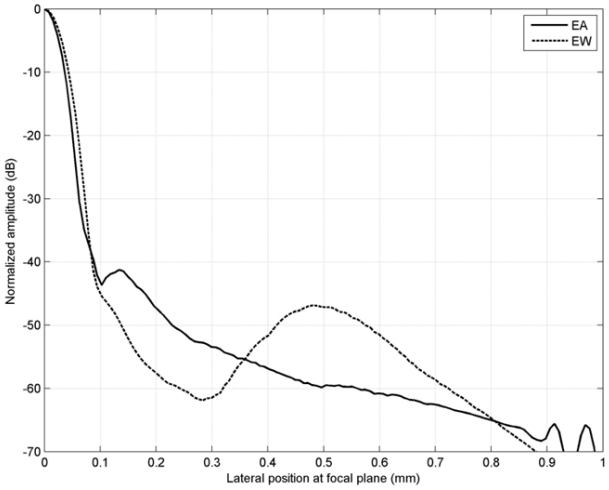

Fig.5:: The radiation patterns of the EA and EW array by using FEA

the grating lobe common in linear arrays, which is very likely due to the linear distribution of annular elements along the EW array aperture. Nevertheless, the level of this grating lobe in the EW array is about -7 dB lower than the sidelobe in the EA array. More importantly, this grating lobe can be further suppressed by inserting more elements into the array, and even moved out from the focal plane if the element pitch of the EW array meets the 1 λ (λ - wavelength) pitch rule for linear arrays [9]. This is due to grating lobes in EW arrays behaving similarly to grating lobes in linear arrays.

Another drawback of the sidelobe suppression in the EW array is the slight decrease in resolution. The resolution of this EW array is found to be 65 μm approximately, 10 μm larger than for the EA array. However, for a conventional 30MHz annular array showing f-number of 2, its resolution is about 100 μm, therefore the strong-focused EW array still shows a significant improvement.

5. CONCLUSION

This paper observes that a strongly-focused annular array can improve imaging resolution without the requirement to increase the operating frequency. A 30 MHz, 5-element, 1 mm EA annular array with f-number of 1 was investigated by using FEA; its resolution was found to be 55 μm approximately, which is almost half of a conventional transducer with an f-number of 2 (100 μm). However, a high sidelobe appears in the region close to the main lobe. A method is then developed to reduce this lobe to avoid any artefacts in the imaging pattern. The close phase difference between adjacent elements is found to be the main reason of this sidelobe; a strong addition is expected for the adjacent pulses emitted from outer elements in the EA array. A change of array geometry can be used suppress this lobe by enlarging the phase difference in outer elements to reduce the chances of

pulse overlap. An EW array is then developed and its radiation pattern successfully shows the sidelobe reduction. However, the cost is the appearance of another lobe, similar in behaviour to a linear array grating lobe. The lobe is -7 dB lower than the sidelobe in EA array, and it can be further suppressed by putting more elements in the EW array. If the element pitch of the EW array is about 1 λ, this grating lobe could be even moved out from the focal plane. In addition, another deficiency of the EW array is the slightly increased resolution compared to the strong-focused EA array, while its value about 65 μm is still much finer than that of the conventional arrays with an f-number of 2 (100 μm). To conclude, this study has shown that geometry modifications to the traditional Equal Area array allows the use of strongly focussed arrays. The significant sidelobes that form as a result of using low F numbers, which compromise imaging performance, have been investigated and the proposed geometry change allows these sidelobes to be controlled. As a result, an Equal Width geometry allows a good compromise between improving the resolution at a given frequency, and allowing sidelobe suppression which would otherwise compromise imaging performance.

References

[1] J. A. Brown, C. E. M. Demore, G. R. Lockwood, "Design and fabrication of annular arrays for high-frequency ultrasound.", *IEEE Transactions on Ultrasonics Ferroelectrics and Frequency Control*, vol. 51, no. 8, pp. 1010-1017, 2004.

[2] K. A. Snook, T. R. Shrout, K. K. Shung, "Development of high frequency annular arrays for medical imaging.", *IEEE International Ultrasonics Symposium*, vol. 1, pp. 865–868, 2003.

[3] K. Snook, T. Shrout, K. K. Shung, "Design of a 50 MHz annular array using fine-grain lead titanate.", 13^{th} *IEEE International Symposium on Applications of Ferroelectrics*, pp. 351–354, 2002.

[4] J. A. Ketterling, O. Aristizabal, D. H. Turnbull, F. L. Lizzi, "Design and fabrication of a 40-MHz annular array transducer.", *IEEE Transactions on Ultrasonics, Ferroelectrics and Frequency Control* , vol 52, no. 4, pp. 672–681.

[5] K. A. Snook, C. H. Hu, T. R. Shrout, K. K. Shung, "High-frequency ultrasound annular-array imaging. Part I: Array design and fabrication.", *IEEE Transactions on Ultrasonics, Ferroelectrics and Frequency Control* , vol. 53, no 2, pp. 300–308, 2006.

[6] C. Passmann, H. Ermert, T. Auer, K. Kaspar, S. el-Gammal, P. Altmeyer, "In vivo ultrasound biomicroscopy.", *IEEE Proceedings Ultrasonics Symposium*, vol. 2, pp. 1015–1018, 1993.

[7] M. J. Zipparo, K. K. Shung, T. R. Shrout, "Piezoceramics for high-frequency (20 to 100 MHz) single-element imaging transducers.", *IEEE Transactions on Ultrasonics, Ferroelectrics and Frequency Control*, vol. 44, no. 5, pp. 1038–1048, 1997.

[8] V. Pasquer, N. Dube, A. Lamarre, "Dynamic focusing of phased arrays for non-destructive testing: Characterization and application.", *Emerging Technologies in NDT.net*, vol. 4, no. 9, pp. 89-95, 1999.

[9] T. L. Szabo, "Diagnostic Ultrasound Imaging: Inside Out, 2^{nd} Edition.", *A volume in Biomedical Engineering, Elsevier Academic Press.*

[10] H. J. Vos, M. E. Frijlink, E. Droog, D. E. Goertz, G. Blacquiere, A. Gisolf, N. de Jong, A. F. W. van der Steen, "A 20-40 MHz ultrasound transducer for intravascular harmonic imaging.", *IEEE Ultrasonics Symposium*, vol 3, pp. 1966–1969, 2004.

[11] S. Michau, P. Mauchamp, R. Dufait, "Piezocomposite 30MHz linear array for medical imaging: design challenges and performances evaluation of a 128 elements array.", *IEEE Ultrasonics Symposium*, vol. 2, pp. 898–901, 2004.

[12] Haifeng Wang, T. A. Ritter, Wenwu Cao, K. K. Shung, "High frequency properties of passive materials for ultrasonic transducers.", *IEEE Transactions on Ultrasonics, Ferroelectrics and Frequency Control*, vol. 48, no. 1, pp. 78–84, 2001.